2022 IEEE International Conference on
Systems, Man, and Cybernetics (SMC)

A Lumped Element Method for Acoustoelectric Imaging Reconstruction: A Numerical Study

Rick Hao Tan
Faculty of Engineering and Applied Science
Ontario Tech University
Oshawa, Canada
hao.tan1@ontariotechu.net

Conor McDermott
Systems and Computer Engineering
Carelton University
Ottawa, Ontario
conor.mcdermott@carelton.ca

Carlos Rossa
Systems and Computer Engineering
Carleton University
Ottawa, Canada
rossa@sce.carleton.ca

2022 IEEE International Conference on Systems, Man, and Cybernetics (SMC) | 978-1-6654-5258-8/22/$31.00 ©2022 IEEE | DOI: 10.1109/SMC53654.2022.9945111

***Abstract*—Acoustoelectric impedance tomography (AET) is a new non-invasive medical imaging procedure used to map the electrical properties of biological tissues with higher spatial resolution than traditional electrical impedance tomography (EIT). It exploits the acoustoelectric effect where modulated ultrasonic pressure changes the local tissue conductivity. This provides additional information to reconstruct a tomographic image, and has a stabilizing effect on an otherwise highly unstable inverse problem.**

In this paper, a novel approach to solving the AET inverse problem for image reconstruction is proposed. In the algorithm, the acoustoelectric effect is assumed to create small perturbations in the local resistance of the medium under observation. A lumped model consisting of a finite mesh of resistors approximates the medium under observation, through which boundary voltage differences between the excited and unexcited medium are calculated. A variation of the Modified Newton Raphson (MNR) algorithm is then proposed, where each pattern in the algorithm is created from small perturbations of the tissue conductivity. A total of eight simulation scenarios are evaluated, where the conductivity perturbations are in the order of 1%, 2.5% to 5% of the nominal tissue conductivity. The algorithm can successfully reconstruct the images in the presence of random noise. The obtained images are compared against traditional EIT where the percentage error is calculated for each simulated tomographic image. The simulation results indicate that the proposed approach is superior to traditional EIT as it constructs more distinct and high contrasting images with less percentage error.

***Index Terms*—Electrical impedance tomography; Ultrasound Imaging; Dual-Modality Imaging; Optimization; Imaging.**

I. Introduction

Electrical impedance tomography (EIT) is a relatively fast, inexpensive and non-invasive imaging procedure. It involves placing electrodes on the surface of the medium being examined [1]. A pair of electrodes then inject electrical current into the medium while the remaining pairs measure and record the resulting boundary voltages. The unique voltage readings are then used to construct a tomographic image of the medium that represents the distribution of its electrical impedance [2]. The use of EIT in medical procedures has been well documented and its applications are vast [3]–[7]. Although EIT is able to provide high contrast tomographic images, its inherent resolution is low due to its ill-posedness of the mathematical inverse problem [2], [8].

Improving the resolution of EIT has been the focus of extensive research over the past few decades. EIT may be complemented with another imaging modality to construct an improved tomographic image [8]. These include fusing MRI and EIT images, developing magnetic resonance electrical impedance tomography (MREIT), gamma densitometry tomography (GDTEIT), ultrasound electrical impedance tomography (UEIT), and acoustic electrical tomography (AET) [8]–[12]. These modalities are often referred to as *multimodal imaging*, that is, the simultaneous production of signals for more than one imaging technique.

On the other hand, *hybrid imaging* fuses two or more imaging techniques into a single, new form of imaging that exploits their coupled physical interaction. Acoustic electric tomography (AET), for example, was developed as an improvement to EIT. The fundamental execution of AET is similar to that of that of EIT. Electrical current is injected into the medium via a pair of boundary electrodes and voltages are measured across the remaining electrodes. An ultrasonic wave is then introduced into the medium under observation and as it propagates, the acoustic pressure elastically deforms a part of the medium. This perturbation induces a small change in the medium's conductivity, in the range of 1% to 5%. This change in conductivity is recorded by the boundary voltages via the peripheral electrodes. Similar to EIT, the resulting unique boundary voltage readings are used to construct a tomographic image of the internal conductivity [12]. This technique results in an increased number of boundary measurements, and hence the ill-posedness of the problem is reduced, leading to potentially higher resolution images [12]. There are various medical applications of hybrid imaging utilizing both ultrasound and EIT. Soleimani performed a study on ultrasound combined EIT for the application of cryosurgery [13]. Other medical applications include lung monitoring and breast tumour detection [14], [15]. The potential applications of hybrid AET imaging is significant and can be further extended to various other medical procedures such as ultrasound focused ovarian cancer detection as well as brachytherapy imaging [16], [17].

The conductivity reconstruction of AET has been solved using various different approaches. Iterative methods using Picard and Newton methods have been documented [18]. Liang et al. used an equality constraint method to solve the reconstruction using a Lagrange-Newton approach [8].

We acknowledge the support of the Natural Sciences and Engineering Research Council of Canada (NSERC), the Canadian Institutes of Health Research (CIHR), and the Social Sciences and Humanities Research Council of Canada (SSHRC), [funding reference number NFRFE-2018-01986].

Cette recherche a été financée par le Conseil de recherches en sciences naturelles et en génie du Canada (CRSNG), par les Instituts de recherche en santé du Canada (IRSC), et par le Conseil de recherches en sciences humaines du Canada (CRSH), [numéro de référence NFRFE-2018-01986]

A common AET approach to reconstructing the conductivity distribution is using power densities [19], [20]. The Levenberg Marquardt method for solving the power density function has been documented in several research works [12], [19], [21]. Its results have been proven to be successful in several different scenarios. Adesokan et al. proposed using a non-linear conjugate gradient optimization for solving the power density [22] while an iterative procedure for solving the power density function using Landweber iteration algorithm is proposed by [23]. These reconstruction algorithms utilize the resulting voltage information obtained from the acoustic excitation directly in the inverse algorithms.

Other reconstruction methods use the spatial information of the inclusion obtained form ultrasound images to sequentially assist in the image reconstruction and convergence in traditional EIT algorithms [24], [25]. In these methods, the boundary voltages of the ultrasound excited medium are not directly utilized in the inverse algorithm and it is a multimodal imaging approach.

Although the aforementioned algorithms are capable of producing tomographic AET images, they have their own drawbacks. Solving the reconstruction problem using the Levenberg Marquardt method is computationally complex as it involves calculating a set of equations for each measurement [12]. Moreover, reconstruction with a conductivity contrast of greater than 5 may destabilize the system [12]. Similarly, the algorithm proposed in [19] requires solving a set of weights during the reconstruction iterative process, which proves to be computationally taxing. The methods proposed in [24], [25] are successful in constructing an accurate tomographic image, however, the boundary voltages from the excited medium are not taken directly into the EIT inverse algorithm. Such information could improve the ill-posedness and resolution of EIT. The algorithms presented in [18], [22], [23] are robust against noise and different inclusion setups, however, their performance comparison to other existing iterative algorithms have not been documented thoroughly.

In this paper, a novel iterative procedure for solving AET is proposed, specifically an equivalent lumped impedance model of the medium is contracted for both the forward and inverse problems and image reconstruction is achieved through a Modified Newton Raphson algorithm (MNR). The MNR algorithm is a robust and popular approach for solving ill-posed inverse problems, especially for EIT [26]. Its performance against other existing inverse algorithms has also been well documented [26]. The algorithm relies on calculating a Jacobian matrix to update an initial conductivity distribution in an iterative fashion until a predetermined end condition has been reached [26]. The algorithm is relatively efficient as it does not need to calculate a system of equations for each AET measurement or a set of weights in the inverse approach.

In the lumped model, the acoustoelectric effect is modelled as a small localized change in one of the model elements, of a group of elements. In the scope of this paper, this change in tissue conductivity is assumed to be ideal, known, and within the range observed in literature. Determining the actual ultrasound/tissue interaction and pressure is beyond the scope of this study. As the localized tissue conductivity perturbations are steered across the medium, the proposed algorithm calculates the resulting boundary voltages, which are then subtracted from voltages measured in the absence of acoustoelectric perturbations. The subtracted voltage values for each perturbation are used in the MNR algorithm to construct a tomographic image. Moreover, the scope of this paper is a simulation study aimed at confirming the principle of the method proposed. Future experiments will follow to confirm the results of this study.

The contributions in this paper include the implementation of Modified Newton Raphson using voltage difference values to solve the problem of AET; and the different patterns used in the MNR algorithm are the lumped ultrasonic excitation patterns instead of traditional EIT electrical current injection patterns. To the best of the author's knowledge, such lumped model combined with AET utilizing MNR has not been proposed for AET. This paper is structured as follows: Section II details the problem of traditional electrical impedance tomography. It is then followed by the explanation of the acoustoelectric effect from the ultrasound excitation. The Modified Newton Raphson algorithm is outlined in Section III. The simulations and the results are displayed in Sections IV,V. The conclusion is presented last in Section VI.

II. Acoustoelectric Impedance Tomography

In order to understand the proposed method for AET image reconstruction, it is important to review the fundamental solution of EIT.

A. Electrical Impedance Tomography

Let the medium under observation be defined as ζ. To perform EIT, electrical current $I(\vec{x})$ is injected into ζ, where $\vec{x}$ is the voxel position within the medium, and $\vec{y}$ are voxel positions on the boundary of the medium. As a result of the injected electrical current, the voltage distribution inside ζ is described by $U(\vec{x})$. The voltages observed by the electrodes on the boundary of ζ is termed as $U_b(\vec{x})$. The conductivity distribution inside ζ is $\sigma(\vec{x})$. To execute both EIT and AET, electrical current is injected in the medium through its boundary $\partial\zeta$, and the goal is to solve for $\sigma(\vec{x})$ [2], [6].

Solving the complete EIT problem usually involves a forward and inverse solution [2]. In the forward solution, the internal conductivity $\sigma(\vec{x})$ is known. The goal is to solve for the boundary voltages U_b for each of the applied current injections $I(\vec{x})$.:

$$U_b(\vec{y}) = f(I(\vec{y}), \sigma(\vec{x})), \ \ \forall \vec{y} \in \partial\zeta \wedge \vec{x} \in \zeta. \tag{1}$$

On the contrary, the boundary voltages $U_b(\vec{x})$ are known for the inverse solution. The goal is to solve for the internal conductivity values $\sigma(\vec{x})$:

$$\sigma(\vec{x}) = f^{-1}(I(\vec{y}), U_b(\vec{y})), \ \ \forall \vec{y} \in \partial\zeta \wedge \vec{x} \in \zeta. \tag{2}$$

Oftentimes, there are far more unknown variables than known variables in the mathematical formulation of the EIT problem. Hence, the problem of EIT is severely ill-posed. To solve the problem of EIT, the forward (1) and the inverse (2) solutions are usually utilized in an alternate fashion in order to reconstruct images in EIT [27]–[30]. In this paper, the problem is expanded to account for variation in the medium conductivity that result from an applied accoustic pressure. This is know as the acoustoelectric effect.

B. The Acoustoelectric Effect

The acoustoelectric effect (AE) describes the change in conductivity within a medium when an ultrasonic pressure is applied to it locally [31]. By defining the initial conductivity of the medium as σ_0, and the material specific AE coupling constant as K [32], [33], the acoustoelectric effect can be stated as [31]:

$$\Delta\sigma = -\sigma_0 K \Delta P, \tag{3}$$

where $\Delta\sigma$ is conductivity change between the perturbed and non-perturbed configurations and P is the amplitude of the pressure waves.

To define the resulting voltage distribution from the acoustoelectric effect, $U_\tau(t_c)$ of the medium at time t_c, the lead field L and time varying current densities ι are established. Using Ohm's Law, $U(t_c)$ is defined as the volumetric integral of L, ι and the initial medium conductivity σ_0 [31]:

$$U_\tau(t_c) = \iiint (L(x,\upsilon,\omega)\cdot\iota(x,\upsilon,\omega,t_c))\sigma_0(x,\upsilon,\omega)\,dxd\upsilon d\omega. \tag{4}$$

The indices x, υ, and ω are the 3D voxel coordinates. By removing the lead field for simplicity and substituting the acoustoelectric effect from (3) into (4), the voltage can be rewritten as:

$$U_\tau = \int\int\int \iota(\sigma_0 - K\sigma_0\Delta P)\,dxd\upsilon d\omega. \tag{5}$$

Close examination of U reveals that the voltage can be further divided into two specific voltages: U_{LF} and U_{AE} [31]:

$$U_\tau = U_{LF} + U_{AE}. \tag{6}$$

In (6), U_{LF} represent the voltage of the medium when no acousto-electric effect is present and is a result of the injected current. In contrast, U_{AE} is the voltage when the ultrasonic pressure propagates through the medium. Using the previously defined terms in (4) and (6), the separate voltages can be further refined as:

$$U_\tau = U_{LF} + U_{AE} = \int\int\int \iota\sigma_0\,dxd\upsilon d\omega - \int\int\int \iota K\sigma_0\Delta P\,dxd\upsilon d\omega. \tag{7}$$

The boundary voltages from the excited medium, U_τ is subtracted from the boundary voltages of the non-excited medium U. The difference in voltage is used in the inverse solution of MNR to solve for the reconstruction, as explained in Section. III.

The approach of using voltage difference between the excited and non-excited medium provides an alternative method of obtaining unique measurements for solving the inverse algorithm. Conductivity perturbations in AET provide an alternative to the current injection patterns of EIT [34]. The ability to obtain sufficient unique voltage measurements with different injection patterns in EIT in order to mitigate the ill-posedness of the inverse problem is limited, whereas in the proposed lump element model, there can be multiple varying acoustic perturbation patterns. This provides the advantage of generating much more unique voltage measurements to mitigate the ill-posedness of the inverse problem.

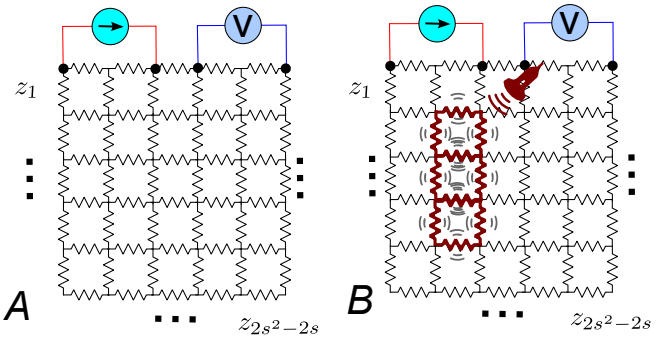

Fig. 1: Different group of resistors are excited using ultrasonic pressure as can be seen in B. The voltages are obtained from the boundary of the mesh. The voltage differences are taken from the boundary of an unexcited mesh (A) and an excited mesh (B).

III. AET Inverse Problem via Modified Newton Raphson

To set up the inverse problem, a set of assumptions need to be defined.

- **Assumption 1**: In (3), it is assumed that the medium specific accoustoelectric coupling constant K is known. This is a common assumption in AET [31];
- **Assumption 2**: The constant ΔP in (3) is known beforehand.
- **Assumption 3**: The area within the medium under observation, and the equivalent area in the lumped model, that are subjected to conductivity changes due to ultrasonic pressure are also known. With these assumptions, the inverse AET image reconstruction problem can be defined.

In order to solve the AET inverse problem, it is first necessary to discretize the medium as a finite lumped model. A finite mesh of resistors is established to represent the medium ζ as shown in Fig. 1. The resistances are labelled as z_β with $1 \leq \beta \leq 2s^2 - 2s$ where s is the total amount of nodes in the resistor grid. An electrical current is applied to a pair of mesh boundary nodes while the induced boundary voltages are measured at n node pairs. In the figure, $n = 1$.

The algorithm begins by recording the n induced voltages $\mathbf{v}_0 \in \mathbb{R}^{n\times 1}$ observed in the absence of any ultrasonic stimulation (Fig. 1 A). Then, the effect of a hypothetical ultrasonic pressure applied to a predefined area of the tissue results in a local change of the tissue resistivity and boundary voltages (Fig. 1 B). All the n voltage are then remeasured. If a number p of ultrasonic patterns is applied to different areas of the tissue, one at a time, there are $n \times p$ unique voltage measurements in the presence of ultrasonic pressure, hereafter denoted as $\mathbf{V}_u \in \mathbb{R}^{n\times p}$. The difference between the perturbed and non-perturbed voltages can now be calculated as:

$$\mathbf{V} = \mathbf{V}_u - \mathbf{v}_0 \circ \mathbf{h} \tag{8}$$

where $\mathbf{h}^{1\times p}$ is a vector of ones, and $\circ$ denotes the Hadarmard product, allowing column-wise subtraction between $\mathbf{V}_u$ and $\mathbf{v}_0$.

The objective of the algorithm is to determine the value of the mesh resistors $\mathbf{z}$ such that the calculated voltage

differences $\hat{\mathbf{V}} \in \mathbb{R}^{n\times p}$ obtained through the lumped model approaches the measured voltages $\mathbf{V}$. The voltage least square error $\theta(\mathbf{z})$ is established according to [26] as:

$$\theta(\mathbf{z}) = \frac{1}{2}\left[\hat{\mathbf{V}}(\mathbf{z}) - \mathbf{V}(\zeta)\right]^T \left[\hat{\mathbf{V}}(\mathbf{z}) - \mathbf{V}(\zeta)\right] \tag{9}$$

In the above, $\mathbf{z} \in \mathbb{R}^{1\times(2s^2-2s)}$ is a vector that holds all the mesh resistors. For each excitation pattern, a lumped group of resistors are excited via (3). The respective resistance values are then updated by setting:

$$\mathbf{z} = \mathbf{z}_0 \circ \mathbf{H}_{ex}. \tag{10}$$

where the vector $\mathbf{z}_0 \in \mathbb{R}^{1\times(2s^2-2s)}$ holds all the resistances in the absence of ultrasonic pressure. The matrix $\mathbf{H}_{ex}$ has a value of 1 in every column, except for the columns corresponding to the resistors being excited by ultrasound. In those columns, the value becomes $(1 - K\Delta P)$ to represent the change in resistance as a result of (3).

The Modified Newton Raphson algorithm is an iterative approach to solving non-linear ill-posed mathematical problems [6], [26]. In order to start the algorithm, an initial resistance distribution is established $\mathbf{z}^o$. Through the algorithm, the initial resistance distribution is updated via the iterations of MNR:

$$\mathbf{z}^{k+1} = \mathbf{z}^k + \Delta\mathbf{z}^k, \tag{11}$$

where k represents the iteration index. The calculated update resistance term, $\Delta\mathbf{z}^k$, is added to $\mathbf{z}^k$ to yield the updated resistance vector $\mathbf{z}^{k+1} \in \mathbb{R}^{1\times(2s^2-2s)}$ at iteration $k+1$. The MNR algorithm will terminate once $\Delta\mathbf{z}^k$ becomes insignificantly small, or if k reaches a predefined value.

Since the objective is to continuously update $\mathbf{z}$ such that $\theta(\mathbf{z}) \to 0$, (9) is to be differentiated with respect to $\mathbf{z}^k$ and set equal to zero [26]:

$$\frac{\partial\theta}{\partial\mathbf{z}^k} = \frac{\partial\hat{\mathbf{V}}^T}{\partial\mathbf{z}^k}[\hat{\mathbf{V}} - \mathbf{V}] = 0, \text{ or} \tag{12}$$

$$\theta' = [\hat{\mathbf{V}}']^T[\hat{\mathbf{V}} - \mathbf{V}] = 0. \tag{13}$$

In (13), the term $\hat{\mathbf{V}}' = \partial\hat{\mathbf{V}}/\partial\mathbf{z}^k \in \mathbb{R}^{(n\times p)\times 2s^2-2s}$ is the Jacobian matrix [26]. The Jacobian defines the rate of change of each boundary voltage reading with respect to each of the resistors in the finite mesh of Fig. 1. In matrix form, the Jacobian is displayed as:

$$[\hat{\mathbf{V}}'] = \begin{bmatrix} \frac{\partial\hat{V}_1}{\partial z_1} & \frac{\partial\hat{V}_1}{\partial z_2} & \cdots & \frac{\partial\hat{V}_1}{\partial z_{2s^2-2s}} \\ \frac{\partial\hat{V}_2}{\partial z_1} & \frac{\partial\hat{V}_2}{\partial z_2} & \cdots & \frac{\partial\hat{V}_2}{\partial z_{2s^2-2s}} \\ \vdots & \vdots & \ddots & \vdots \\ \frac{\partial\hat{V}_{n\times p}}{\partial z_1} & \cdots & \cdots & \frac{\partial\hat{V}_{n\times p}}{\partial z_{2s^2-2s}} \end{bmatrix}. \tag{14}$$

Since (13) is a non-linear function of $\mathbf{z}^k$, the equation is rewritten by taking the Taylor Series Expansion about an arbitrary point $\mathbf{z} = \mathbf{z}^k$ [26] to yield:

$$\theta' \approx \theta'(\mathbf{z}^k) + \theta''(\mathbf{z}^k)\Delta\mathbf{z}^k. \tag{15}$$

in which $\theta'' = \partial^2\hat{\mathbf{V}}/\partial\mathbf{z}^2$ is the Hessian matrix [26], and it can be represented as:

$$\theta'' \approx [\hat{\mathbf{V}}']^T[\hat{\mathbf{V}}']. \tag{16}$$

Finally, the solution for $\Delta\mathbf{z}^k$ can then be calculated by substituting (13) and (16) into (15) to yield:

$$\Delta\mathbf{z}^k = \tag{17}$$
$$-\left\{[\hat{\mathbf{V}}'(\mathbf{z}^k)]^{\mathbf{T}}\hat{\mathbf{V}}'(\mathbf{z}^k) + \lambda\mathbf{W}\right\}^{-1}[\hat{\mathbf{V}}'(\mathbf{z}^k)][\hat{\mathbf{V}}(\mathbf{z}^k) - \mathbf{V}].$$

In (17) the Marquardt method is implemented to mitigate the ill-conditioning [26], [35]. The matrix, $\mathbf{W}$, is an identity matrix multiplied by the scalar $\lambda \in \mathbb{R}^+ \to 0$. Both terms $\mathbf{W}$ and λ prevent the system from reaching singularity. The smaller the λ value, the more accurate the inverse solution is. The overall MNR procedure is schematized in Fig. 2.

The final solution will heavily depend on the initial resistance estimation. In the study conducted by Murai and Kagawa, it is claimed that a solution will converge if $|\mathbf{z^0} - \mathbf{z_t}| < 10$ [36], with $\mathbf{z_t}$ being the true resistance distribution.

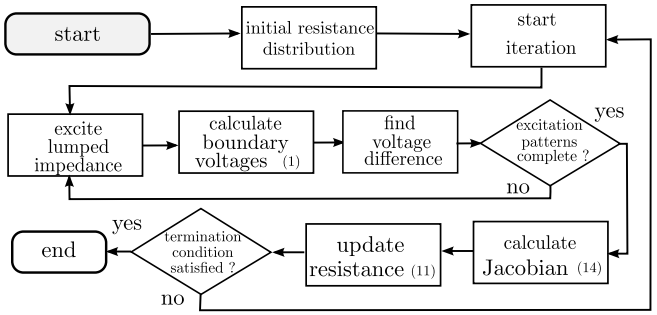

Fig. 2: The overall workflow of the MNR algorithm. The iterative procedure repeats until a termination condition is satisfied.

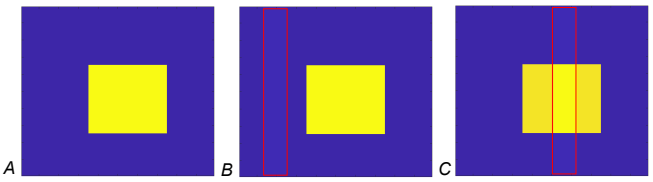

Fig. 3: In A, the baseline distribution is established with the centre inclusion at 40 Ω and the background at 10 Ω. In B and C, the tissue conductivity is perturbed vertically along the mesh to simulate the acoustoelectric effect.

IV. Forward and Inverse AET Simulation

The **forward problem** or the true conductivity distribution, is established on a mesh of 50×50 nodes in a square fashion with 4,900 resistor elements, as shown in Fig. 3 A. The true distribution has background values of 10 Ω and the inclusion to be identified is configured at 40 Ω. The electrical current is injected in a fixed location, entering the top left corner of the conductivity mesh and leaving at the bottom right corner. In total, voltages are measured at 13 distinct points along the boundary of the medium using adjacent measurement patterns [34]. A random noise of up to 2% is introduced into the boundary voltage readings.

The acoustoelectric effect is modulated through 8 excitation patterns. It is assumed that a hypothetical and ideal unfocused ultrasonic wave changes the resistivity of a vertical strip of resistors as shown in Fig. 3 B-C, covering from the top of the mesh to the bottom of the mesh. The maximum

change in resistivity used in the simulations, as given in given in (3), varies from 1%, 2.5%, to 5%. The variance percentages were selected as it corresponds to the level observed experimentally in [37].

The **inverse problem** is performed on a mesh of 26×26 nodes with 1,300 resistor elements. A total of eight scenarios are simulated: six AET simulations and two EIT simulation for comparison. **Scenarios 1 to 3**: The AET simulations are performed with local conductivity variations increasing from 1%, 2.5% to 5% respectively. A large inclusion is placed in the centre. **Scenario 4**: A pure traditional EIT simulation solved with MNR with 8 current injection patterns with 13 voltage measurements each on the centre inclusion distribution. **Scenarios 5 to 7**: The AET simulations are performed with local conductivity variations increasing from 1%, 2.5% to 5% respectively. A small inclusion is placed in the bottom right corner. **Scenario 8**: A pure traditional EIT simulation solved with MNR with 8 current injection patterns with 13 voltage measurements each on the bottom right inclusion distribution.

There is a total number of 104 unique voltage measurements in both the AET simulations and EIT. For the MNR algorithm, a total of k = 3 iterations are implemented with $1 \times 10^{-11} < \lambda < 1 \times 10^{-9}$. The results for the different scenarios are shown in the following section.

V. Simulation Results and Discussion

The simulation results are displayed in Fig. 4, where the *conductivity* images are normalized on a scale of 0 to 1. The gradient of colours indicate the difference in conductivity identified. In all of the AET simulations, the proposed algorithm is proven to be effective while the mesh is administered with different perturbation levels. The centre inclusion of 40 Ω is identified successfully while contrasted against the background of 10 Ω. Furthermore, the proposed approach is robust against the injected noise of 2%.

In order to quantitatively compare the obtained tomographic images with their true distribution, the percentage error (PE) is calculated. First, the true resistance distribution is reconstructed using a 26x26 mesh as a baseline to allow exact resistor comparison with the calculated resistance distribution. The error is then given as:

$$PE = \sum_{j=1}^{2s^2-2s} \frac{|\hat{\mathbf{z}_j} - \mathbf{z}_{tj}|}{\mathbf{z}_{tj}}, \tag{18}$$

where $\hat{\mathbf{z}}$ is the vector holding all calculated resistance values. The results in Table 1 show that the AET algorithm outperforms traditional EIT as the PE values of all AET Scenarios (1-3, 5-7) are lower than that of the traditional EIT (Scenarios 4 and 8). In Scenarios 1-3, where the inclusion is in the centre, AET is able to define an inclusion with sharp boundaries. Similarly, in Scenarios 5-8, AET is again able to define the corner inclusion with sharp boundaries even with a smaller sized inclusion. In both Scenarios 4 and 8, EIT is able to identify the inclusion, however, there is significant noise in the reconstructed background. The higher percentage error of the EIT reconstruction is a result of the noise present in the background of the images.

TABLE I: Percentage error (PE) between the calculated and true distribution of each simulated scenario (Sc).

	1% AET	2.5% AET	5% AET	EIT
	Sc. 1	Sc. 2	Sc. 3	Sc. 4
PE	0.0824	0.0945	0.0891	0.1223
	Sc. 5	Sc. 6	Sc. 7	Sc. 8
PE	0.0077	0.0124	0.0144	0.0183

VI. Conclusions

In this paper, a novel method of performing AET utilizing a lumped element method with the Modified Newton Raphson technique is proposed. The resistance of different groups of resistors in the lumped model are disturbed to simulate the acoustoelectric effect, with an excitation level ranging from 1%, 2.5% to 5%. The boundary voltages of the excited medium is recorded under random noise. The voltage is then subtracted from the boundary voltages of an identical but unexcited medium. The conductivity disturbance patterns and the voltage difference values are used in the MNR algorithm to perform the image reconstruction. A variation of the MNR for solving AET is proposed, where the local resistivity distribution in the inverse problem is also altered to represent the acoustoelectric effect.

The percentage error calculated for the final tomographic images indicate that the proposed method is superior to traditional EIT. As can be observed from the results displayed, the EIT reconstructed image yielded blurred concentration of the inclusions, whereas the proposed AET algorithm provided more distinct and high contrast images of the inclusion. For future studies, additional excitation levels as well as physical experiments will be conducted to confirm the results provided in this paper.

References

[1] N. Hyvönen, H. Majander, and S. Staboulis, "Compensation for geometric modeling errors by positioning of electrodes in electrical impedance tomography," *Inverse Problems*, vol. 33, no. 3, p. 23, 2017.

[2] J. K. Seo, *Nonlinear inverse problems in imaging*. Chichester, West Sussex, U.K: John Wiley Sons Inc.

[3] P. Blankman, D. Hasan, M. Mourik, and D. Gommers, "Ventilation distribution measured with eit at varying levels of pressure support and neurally adjusted ventilatory assist in patients with ali," *Intensive Care Medicine*, vol. 39, no. 6, pp. 1057–1062, 2013.

[4] E. K. Murphy, A. Mahara, and R. J. Halter, "Absolute reconstructions using rotational electrical impedance tomography for breast cancer imaging," *IEEE Transactions on Medical Imaging*, vol. 36, no. 4, pp. 892–903, 2017.

[5] J. Hough, A. Shearman, H. Liley, C. Grant, and A. Schibler, "Lung recruitment and endotracheal suction in ventilated preterm infants measured with electrical impedance tomography," *Journal of Paediatrics and Child Health*, vol. 50, no. 11, pp. 884–889, 2014.

[6] R. H. Tan and C. Rossa, "Electrical impedance tomography using differential evolution integrated with a modified newton raphson algorithm," in *2020 IEEE International Conference on Systems, Man, and Cybernetics (SMC)*, 2020, pp. 2528–2534.

[7] M. Alsaker, D. A. C. Cárdenas, S. S. Furuie, and J. L. Mueller, "Complementary use of priors for pulmonary imaging with electrical impedance and ultrasound computed tomography," *Journal of Computational and Applied Mathematics*, vol. 395, p. 113591, 2021.

[8] G. Liang, S. Ren, S. Zhao, and F. Dong, "A lagrange-newton method for eit/ut dual-modality image reconstruction," *Sensors (Basel, Switzerland)*, vol. 19, no. 9, pp. 1966–, 2019.

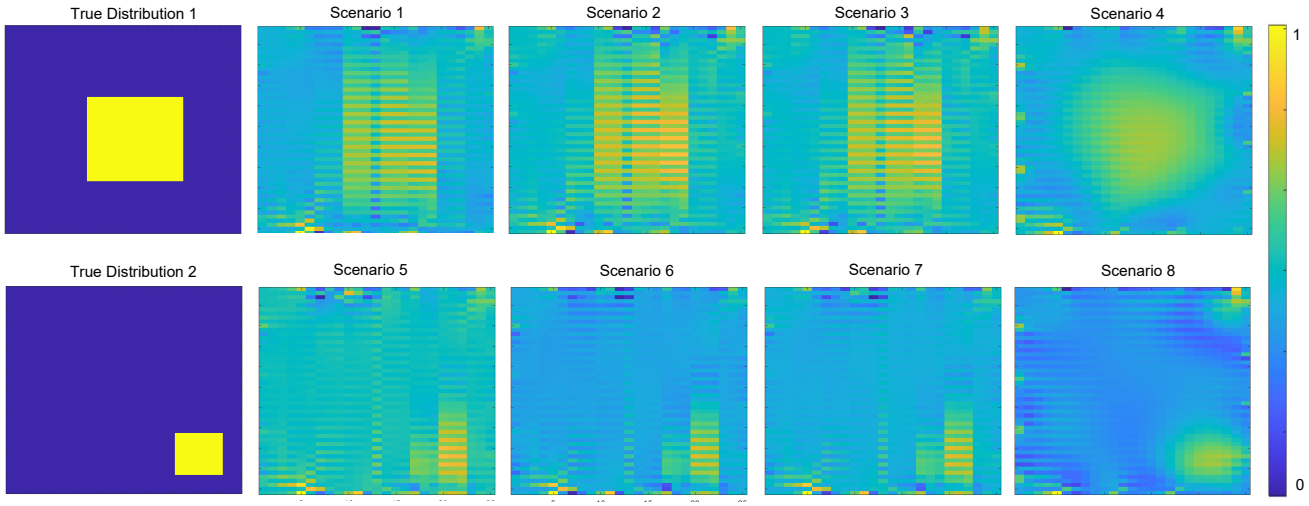

Fig. 4: Scenarios 1-3 and 5-7 demonstrate the proposed AET results with the ultrasound excitation varied: 1%, 2.5% and 5% respectively. Scenarios 4 and 8 are traditional EIT simulations solved with MNR. All simulations are able to successfully construct a conductivity distribution identifying the focal inclusion.

[9] J. L. Davidson, R. A. Little, P. Wright, J. Naish, R. Kikinis, G. J. M. Parker, and H. McCann, "Fusion of images obtained from eit and mri," *Electronics letters*, vol. 48, no. 11, pp. 617–618, 2012.

[10] C. Göksu, K. Scheffler, P. Ehses, L. G. Hanson, and A. Thielscher, "Sensitivity analysis of magnetic field measurements for magnetic resonance electrical impedance tomography (mreit)," *Magnetic resonance in medicine*, vol. 79, no. 2, pp. 748–760, 2018.

[11] G. Johansen and E. Åbro, "A new cdznte detector system for low-energy gamma-ray measurement," *Sensors and actuators. A. Physical.*, vol. 54, no. 1, pp. 493–498, 1996.

[12] C. Li, K. An, and K. Zheng, "The levenbergmarquardt method for acousto-electric tomography on different conductivity contrast," *Applied sciences*, vol. 10, no. 10, pp. 3482–, 2020.

[13] M. Soleimani, "Electrical impedance tomography imaging using a priori ultrasound data," *BioMedical Engineering OnLine*, 2006.

[14] V. Tomicic and R. Cornejo, "Lung monitoring with electrical impedance tomography: technical considerations and clinical applications," *Journal of thoracic disease*, vol. 11, no. 7, pp. 3122–3135, 2019.

[15] G. Steiner, M. Soleimani, and D. Watzenig, "A bio-electromechanical imaging technique with combined electrical impedance and ultrasound tomography," *Physiological measurement*, vol. 29, no. 6, pp. S63–S75, 2008.

[16] R. Wu, B. Hu, L.-X. Jiang, Y. Hung, S.-L. Kuang, and B. Zhang, "High-intensity focused ultrasound in ovarian cancer xenografts," *Advances in therapy*, vol. 25, no. 8, pp. 810–819, 2008.

[17] H. Tan and C. Rossa, "Electrical impedance tomography for robot-aided internal radiation therapy," *Frontiers in Bioengineering and Biotechnology*, vol. 9, p. 698038, 06 2021.

[18] K. Hoffmann and K. Knudsen, "Iterative reconstruction methods for hybrid inverse problems in impedance tomography," *Sensing and imaging*, vol. 15, no. 1, pp. 1–27, 2014.

[19] B. J. Adesokan, B. Jensen, B. Jin, and K. Knudsen, "Acousto-electric tomography with total variation regularization," *Inverse problems*, vol. 35, no. 3, pp. 35 008–, 2019.

[20] H. Ammari, E. Bonnetier, Y. Capdeboscq, M. Tanter, and M. Fink, "Electrical impedance tomography by elastic deformation," *SIAM journal on applied mathematics*, vol. 68, no. 6, pp. 1557–1573, 2008.

[21] L. Changyou, K. Mirza, S. Ekaterina, and K. Kim, "Levenbergmarquardt algorithm for acousto-electric tomography based on the complete electrode model," *Journal of mathematical imaging and vision*, vol. 63, no. 4, pp. 492–502, 2021.

[22] B. J. Adesokan, K. Knudsen, V. P. Krishnan, and S. Roy, "A fully nonlinear optimization approach to acousto-electric tomography," *Inverse problems*, vol. 34, no. 10, pp. 104 004–, 2018.

[23] S. Hubmer, K. Knudsen, C. Li, and E. Sherina, "Limited-angle acousto-electrical tomography," *Inverse problems in science and engineering*, vol. 27, no. 9, pp. 1298–1317, 2019.

[24] K. Ain, D. Kurniadi, S. Suprijanto, and O. Santoso, "Dual modality electrical impedance and ultrasound reflection tomography to improve image quality," *Journal of electrical bioimpedance*, vol. 8, no. 1, pp. 3–10, 2017.

[25] M. Soleimani, "Electrical impedance tomography imaging using a priori ultrasound data," *Biomedical engineering online*, vol. 5, no. 1, pp. 8–8, 2006.

[26] T. J. Yorkey, J. G. Webster, and W. J. Tompkins, "Comparing reconstruction algorithms for electrical impedance tomography," *IEEE Transactions on Biomedical Engineering*, vol. BME-34, no. 11, pp. 843–852, Nov 1987.

[27] J. Padilha Leitzke and H. Zangl, "A review on electrical impedance tomography spectroscopy," *Sensors (Basel, Switzerland)*, vol. 20, no. 18, pp. 5160–, 2020.

[28] W. Q. Yang and L. Peng, "Image reconstruction algorithms for electrical capacitance tomography," *Measurement science technology*, vol. 14, no. 1, pp. R1–R13, 2003.

[29] W. R. B. Lionheart, "Eit reconstruction algorithms: pitfalls, challenges and recent developments," *Physiological measurement*, vol. 25, no. 1, pp. 125–142, 2004.

[30] M. Neumayer, H. Zangl, D. Watzenig, and A. Fuchs, "Current reconstruction algorithms in electrical capacitance tomography," in *New Developments and Applications in Sensing Technology*, ser. Lecture Notes in Electrical Engineering. Berlin, Heidelberg: Springer Berlin Heidelberg, 2011, pp. 65–106.

[31] C. Preston, A. M. Alvarez, A. Barragan, J. Becker, W. S. Kassof, and R. S. Witte, "High resolution transcranial acoustoelectric imaging of current densities from a directional deep brain stimulator," *J Neural Eng*, vol. 17, Feb 2020.

[32] J. Jossinet, B. Lavandier, and D. Cathignol, "Impedance modulation by pulsed ultrasound," *Annals of the New York Academy of Sciences*, vol. 873, no. 1, pp. 396–407, 1999.

[33] Q. Li, R. Olafsson, P. Ingram, Z. Wang, and R. Witte, "Measuring the acoustoelectric interaction constant using ultrasound current source density imaging," *Physics in medicine biology*, vol. 57, no. 19, pp. 5929–5941, 2012.

[34] H. Rajaguru, P. Rathinam, and R. Singaravelu, "Electrical impedance tomography (eit) and its medical applications: a review," *Int J Soft Comp Eng*, vol. 3, pp. 193–8, 01 2013.

[35] D. W. Marquardt, "An algorithm for least-squares estimation of nonlinear parameters," *Journal of the Society for Industrial Applied Mathematics*, vol. 11, no. 2, pp. 431–441, 1963.

[36] T. Murai and Y. Kagawa, "Electrical impedance computed tomography based on a finite element model," *IEEE Transactions on Biomedical Engineering*, vol. BME-32, no. 3, pp. 177–184, March 1985.

[37] B. Lavandier, J. Jossinet, and D. Cathignol, "Quantitative assessment of ultrasound-induced resistance change in saline solution," *Medical biological engineering computing*, vol. 38, no. 2, pp. 150–155, 2000.